WIND TUNNEL TEST OF TWO ELECTRICAL LIFT THRUST UNITS TO ASSESS STATIC AND DYNAMIC LOADS

Davide Balatti, Leonardo Helicopters, Yeovil, UK
Michele Zilletti, Andrea Duina, Mirko Zaccara, Alberto Dispenza, Leonardo Helicopters, Samarate, Italy
Pierangelo Masarati, Politecnico di Milano, Italy

Abstract

The aeronautical community is showing increasing interest in innovative multi-propeller electric Vertical Take-Off and Landing (VTOL) aircraft for Advanced Air Mobility. This paper aims to contribute to the development of new methodologies and tools for assisting in the design of such aircraft from the early stages of their design. Specifically, the paper focuses on developing an experimental wind tunnel test rig to evaluate the static and dynamic loads produced by two electric Lift Thrust Units (eLTUs) under different flight conditions. The test rig measures all six static and dynamic load components in the fixed reference frame produced by each LTU while controlling the rotor speed. The experimental measurement data are correlated with an aeroelastic numerical model and used to explore the aerodynamic and structural interactions of the two LTUs. The introduction of an elastic support, at the base of the LTUs, was shown to be effective in improving the dynamic loads' correlation.

1. INTRODUCTION

The introduction of electrical propulsion systems in rotary-wing aircraft has expanded the design possibilities for new vehicle architectures. Both traditional aerospace industries and emerging companies have invested in developing Vertical Take-Off and Landing (VTOL) aircraft to leverage the benefits of distributed electrical propulsion systems. Researchers at NASA have compared various generic VTOL architectures that incorporate key Urban Air Mobility (UAM) features and technologies, including propulsion architectures, highly efficient and quiet rotors, and enhanced aircraft aerodynamic performance [1, 2]. These new architectures offer several potential advantages, such as increased safety due to the redundancy of the propulsion system, zero emissions with fully electrical power systems, and a reduced number of drive system components, potentially lowering production and maintenance costs and promising increased reliability. One possible simplification of the propulsion system involves the use of multiple Lift/Thrust Units (LTUs) to provide differential thrust for aircraft control, thereby eliminating the need for traditional control mechanisms like swashplates, control chains, and propeller blade pitch control.

Furthermore, the wide operational speed and torque ranges of electric motors mean that only a gearbox with fewer stages between the motor and the propeller may be required, significantly reducing weight compared to the multi-stage traditional combustion engine drive systems. Additionally, the fast response of electric motors allows for thrust regulation of each LTU by controlling the rotor speed, eliminating the need for blade pitch control as in traditional aircraft propellers or helicopter rotors' collective pitch control. Rotor speed control can simplify the LTU design, enabling the use of stiff propellers instead of articulated rotors, thereby reducing the number of rotor components. However, these design features introduce new challenges for designers, including control logic, structural design of the propeller, hub, and airframe, aeroelastic stability, and failure handling, all of which should be addressed from the early design stage.

Articulated rotors in helicopters reduce the dynamic loads transmitted to the rotor hub, whereas stiff propellers are expected to produce higher dynamic loads due to the rigid connection of the blades to the rotor hub. Moreover, the LTU's variable rotor speed control strategy may cause it to operate in a continuous range of RPMs that includes multiple resonance frequencies of the vehicle, amplifying vibratory loads. Therefore, it is crucial to predict the static and dynamic loads generated by an LTU in various flight conditions to guide the design of the LTU, its supporting structure, and the entire airframe.

Recently, researchers have tackled this problem both experimentally and numerically. Russell et al. [3] modelled a small-scale LTU to determine the fidelity needed for accurate performance prediction, using the helicopter comprehensive analysis tool CAMRAD II to correlate wind tunnel test data for a single LTU. Their analysis focused on LTU performance rather than dynamic load prediction. More recently, NASA designed a specialized wind tunnel test bed to assess the performance and dynamic load generation of six LTUs supported by a beam structure [4, 5]. This setup is fully reconfigurable, allowing each LTU to be independently tilted and moved horizontally and vertically. Each LTU was equipped with a load cell to measure the six load components in the fixed reference frame. Sekula et al. [6] conducted a parametric study on the LTU transient response, validating analytical models against NASA's experimental data [5] and emphasizing the importance of the rotor wake model and blade elasticity properties. Shastry et al. [7] developed an analytical model to predict structural loads in multi-rotor eVTOLs, focusing on transient and inharmonic wake interactions from multiple rotors. Staruk et al. [8] tested a full-scale two-blade LTU (1.8 m diameter) in a wind tunnel, observing high dynamic loads generated by the LTU in edgewise rotor airflow conditions.

Zilletti et al. [9] designed and tested a setup to characterize the static and dynamic behaviour of an electrical LTU. Their results showed that a stiff rotor could generate high oscillatory loads in edgewise airflow conditions, with magnitudes comparable to the corresponding static loads. Additionally, they emphasized that the test rig should be designed to avoid any intrusive dynamics. Building on the study presented in Ref. [9], this paper presents the design and testing of a wind tunnel test rig to dynamically characterize two LTUs under various flight conditions and configurations. Section 2 discusses the test rig's design while Section 3 describes the wind tunnel tests. Section 4 details the development of the aeroelastic model using Leonardo Helicopter Division’s (LHD) in-house software, GyroX3 [10]. Sections 5 and 6 cover the initial static and dynamic numerical-experimental correlation. Finally, Section 7 provides the conclusions and outlines future steps.

2. TEST RIG DESIGN

This section presents the design of a two-LTUs wind tunnel test rig capable of measuring the six load components generated by each LTU in the fixed reference frame. The test can be conducted under various flight conditions, characterized by different wind speeds, structure tilt angles, and rotor speeds of each LTU. The main objective of this study is to validate a methodology to predict the static and dynamic loads of electrical LTUs considering possible aerodynamic and structural interactions. Off-the-shelf parts have been used for the test rig, minimizing both time and budget.

The experimental tests were carried out at the LHD wind tunnel facility in Bresso, Italy. The tunnel is a closed-return, 2 m diameter by 2.5 m length single circuit, open jet test section type, with a contraction ratio of 5.18, equipped with a 400 kW – 1200 RPM electric motor and a ten constant-pitch blade fan (2.9 m diameter), which generates typical and max wind speeds of 50 and 65 m/s, respectively (unit length Reynolds number up to $4 \cdot 10^6$ 1/m), with a turbulence factor 1.173%. The airstream quality is improved by installing turning vanes at each circuit corner and a single honeycomb at the settling chamber entrance. No heat exchanger is present, which limits operations up to 45° C. For this experiment, the maximum wind speed was 18 m/s.

Figure 1 shows a picture of the wind tunnel test rig consisting of two LTUs arranged in tandem configuration, supported by an aluminium beam. The supporting structure is mounted on a pylon, which allows it to tilt in the wind direction. The two thrust units can be independently moved along the supporting structure to adjust the distance between the rotors as required. Each LTU consists of a 3-blade fixed pitch angle propeller, approximately 0.6 meters in diameter, driven by an electric motor. An Electronic Speed Controller (ESC) powers the motor, receiving DC power voltage from a power supplier. The rotor speed can

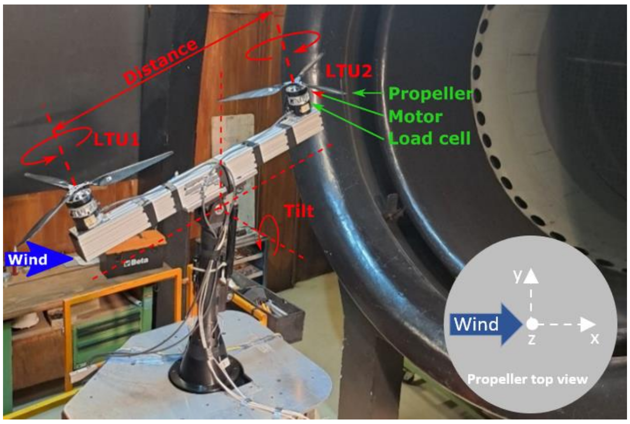

Figure 1: Wind tunnel test rig.

be set through the duty cycle of a Pulse Width Modulated (PWM) signal sent to the ESC. An external control loop has been implemented on an STM32 microcontroller, to regulate the rotor speed under various flight conditions. The microcontroller implements a Proportional Integral Derivative (PID) feedback control, which uses the rotor speed measured by the Hall effect encoder and the desired rotor speed value as inputs and outputs the PWM duty cycle. Figure 2 shows a scheme of the setup's electrical connection.

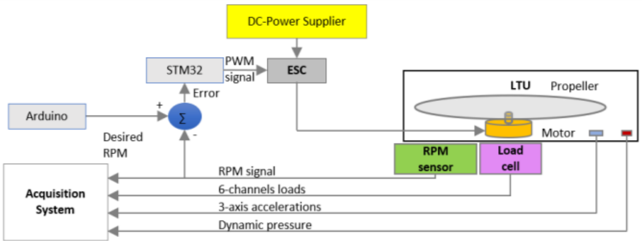

Figure 2: Electrical connection setup.

2.1 Wind tunnel test rig dynamic test

The aluminium supporting structure was initially designed to minimize its impact on the system dynamics and the generation of dynamic loads by the propellers. However, due to the wide frequency excitation band generated by the propellers, it has been challenging to design the structure without resonances within the frequency band of interest while maintaining a reasonable size and weight. After the rig's installation in the wind tunnel, a hammer identification test has been performed to characterize its dynamics.

Figure 3 shows, as an example, the Bode plot of the transfer function between a lateral force and acceleration (left plots) and a vertical force and acceleration (right plots). The forces were applied at the base of the rear LTU while the accelerations were measured with a 3-axial accelerometer at the same location. The transfer function exhibits several resonances with phase angles between 0° and 180°, because of the collocation of force and acceleration.

Table 1 summarizes the natural frequencies, and damping ratio, and provides qualitative descriptions of the mode shapes. The first six modes are rigid modes of the test setup, associated with the deformation of the wind tunnel platform base supporting the pylon. The seventh and eighth modes are related to the pylon support and the rigid motion of the LTU supporting structure. The remaining high-frequency modes are associated with pylon bending modes coupled with the LTUs supporting structure bending vertical, lateral and torsional modes.

Table 1: Test rig resonance frequency and damping ratio, frequencies normalised to the 1st resonance value.

Mode description	Mode	Normalised frequency	Damping ratio
Modes associated to the motion of the wind tunnel platform supporting the pylon	1	1.00	1.52%
	2	1.20	1.29%
	3	1.25	2.34%
	4	1.48	1.24%
	5	1.71	2.02%
	6	2.11	1.12%
Longitudinal pylon bending associated with a rigid pitch of the LTU supporting beam	7	3.94	2.71%
Lateral pylon bending associated with a rigid pitch of the LTU supporting beam	8	4.82	2.48%
Pylon bending associated with vertical, lateral and torsional modes of the LTU supporting beam	9	5.27	3.39%
	10	5.62	1.76%
	11	6.17	2.25%
	12	6.45	0.84%
	13	6.87	1.72%
	14	9.24	1.24%
	15	9.77	0.39%
	16	9.92	0.46%

3. WIND TUNNEL TESTS

For the test campaign, 168 conditions were tested, comprising no wind and 18 m/s wind speed conditions, 3 tilt angles, 3 LTU distances (measured as the distance between the LTUs rotor centre, symmetrically positioned along the beam), and 14 rotor speed steady-state regimes, as summarized in Table 2. In this work, the LTU distances are also expressed as

Table 2: Wind tunnel condition test matrix.

Wind speed [m/s]	Distance [m]	Tilt angle [°]	Rotor speed
0 (only 0° tilt)	0.7 (d/D =1.2)	0	25%
18	0.8 (d/D =1.3)	10	31%
	0.9 (d/D =1.4)	20	38%
			44%
			50%
			56%
			63%
			69%
			75%
			81%
			88%
			94%
			100%
			106%

the ratio of the distance between the LTU's rotor centre (d) and the rotor diameter (D).

In all tested configurations, both LTUs operated at the same rotor speed. The rig was designed to position the LTUs in either a tandem arrangement along the wind direction (as shown in Figure 1) or side-by-side. This paper presents results only for the tandem configuration, where the wake of the front rotor interacts with the rear rotor. In the side-by-side configuration, the two rotors are nearly aerodynamically independent, making this setup less relevant for the purposes of this study. However, in both configurations, the LTUs experience structural interaction, affecting the dynamic loads transmitted to the supporting structure.

During the test, the following signals were acquired using the QuantumX acquisition system: two 6-axis load measurements, wind tunnel dynamic pressure, 3-axis accelerations at the base of each load cell location, and the rotor speed of both propellers. Data acquisition was performed after reaching steady-state wind and rotor speed conditions. Each acquisition lasted 30 seconds with a sampling frequency of 5 kHz. The signals were then post-processed to obtain the static load component (i.e., the mean value of the load time history) and the harmonic component at the 3/rev frequency (i.e., the blade passing frequency) by computing the FFT of the measured signals. The loads of each LTU are referred to a coordinate system with its origin (O) located at the hub centre, the x and z axes aligned with the wind direction and LTU thrust, respectively, and the y-axis perpendicular to the wind direction, forming a right-hand reference system, as shown before in Figure 1.

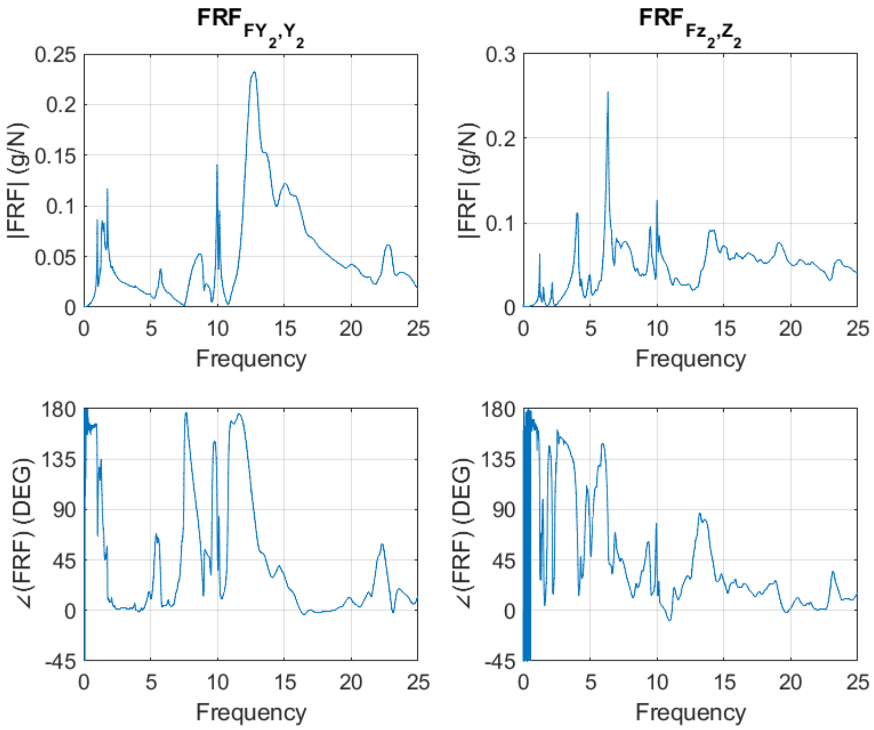

Figure 3: FRF between the vertical force at the hub and the acceleration at the base of the LTU. Frequencies normalised to the 1st resonance value.

4. AEROELASTIC MODEL

In a previous paper, Zilletti et al. [11] presented the propeller characterization and the GyroX3 model definition and validation in the case of a single LTU. The following section presents a summary of the LTUs model definition.

The aeroelastic model of the LTUs was built in GyroX3, an LHD in-house code [10]. Both LTUs share the same structural and aerodynamic model. The only difference between the two LTUs is the rotation direction (looking from the top view, the front rotor counterclockwise and the rear rotor clockwise). The airfoil geometry was obtained through 3D blade scanning, and the aerodynamic coefficients (lift, drag, and pitching moment) were defined as functions of the airfoil angle of attack and Mach number. To create look-up tables for these coefficients, a 2D quadrilateral O-grid mesh was generated using Pointwise®, with pressure far-field boundary conditions and adiabatic wall conditions on the airfoil surface. SST k-ω turbulence models were employed for simulations conducted with Ansys Fluent® at a Reynolds number over Mach number of 6,256,000. The aerodynamic coefficients were then formatted according to the C81 table standard.

Each blade is modelled using 22 beam elements with cubic shape functions, as shown in Figure 4 (the blue spherical markers represent the nodes between the beam elements). The three blades are connected to a shaft via three quasi rigid beams representing the rotor hub. The shaft is modelled as a rigid element with one terminal connected to the rotor hub centre and the other end to the ground. Using the C81 tables obtained via CFD, a Lifting Line free wake model was chosen for the aeroelastic simulation. In detail, the rotor of each LTU was modelled using a standard vortex panel wake. The blade aerodynamic mesh was made of 30 panels with geometrical progression and refinement at the tip. The aerodynamic model was set up so that the aerodynamics and wake of each LTU interact with those of the other LTU. Due to the complex aerodynamic propeller interaction, for each LTU distance, a parametric study was performed to ensure the correct rotor wake size was considered. Indeed, Figure 5a presents a typical aerodynamic solution for the LTUs in a tandem configuration at 0° tilt angle, 18 m/s wind speed and 0.7 m rotors distance, with the wake of the front propeller investing the rear propeller. Figure 5b shows the aerodynamic solution in hover with the first vortex rolling up and the near-wake narrowing just under the rotor plane.

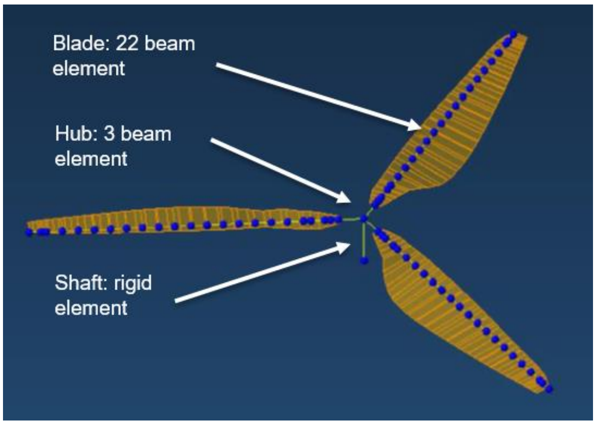

Figure 4: GyroX3 rotor model.

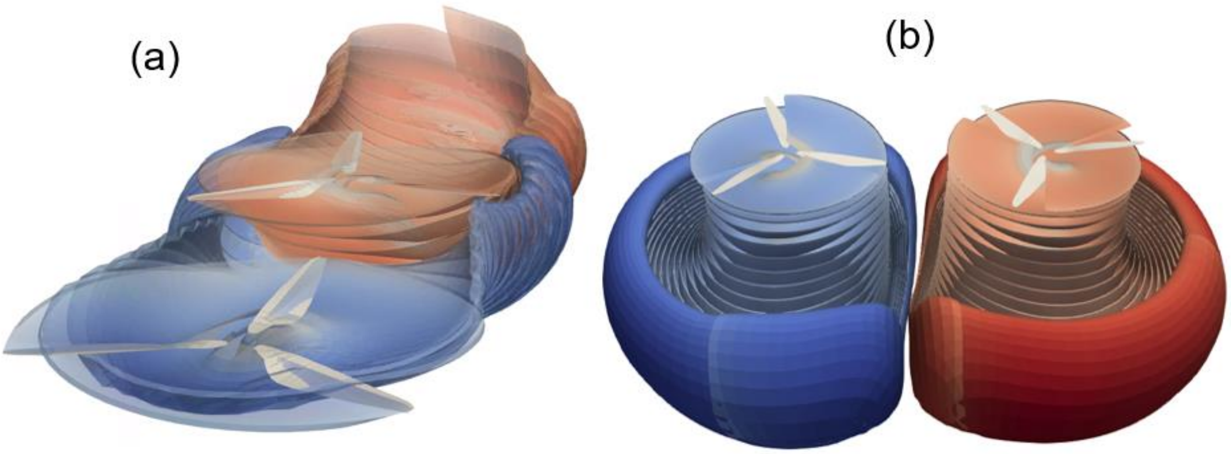

Figure 5: Typical aerodynamic solution in (a) in tandem configuration at 18 m/s, 0° tilting angle and 0.7 m rotors distance with the wake of the front LTU investing the rear LTU and (b) hover with the first vortex rolling up and the near-wake narrowing just under the rotor plane.

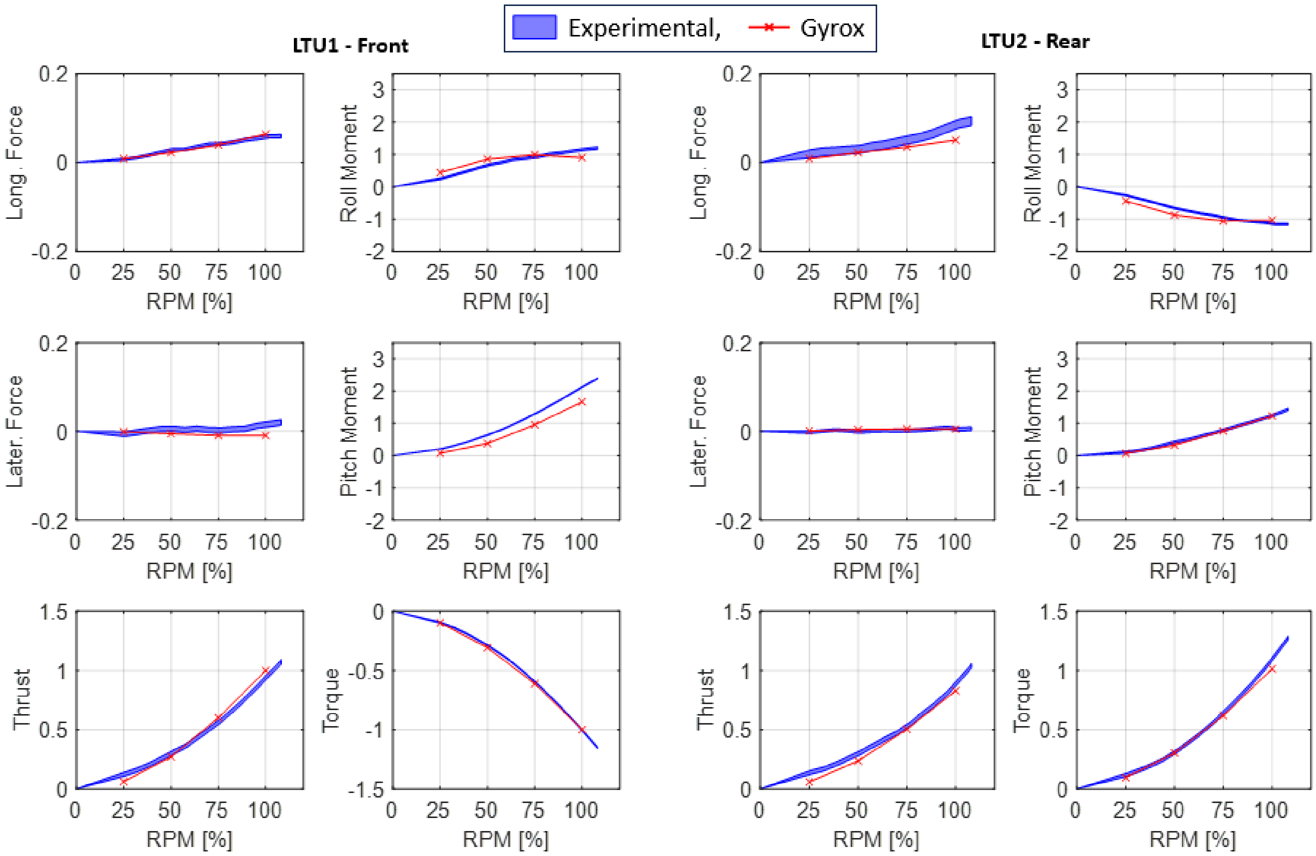

Figure 6: Measured (blue area) and simulated (red line) static forces and moments as a function of the rotor speed. Test condition: 10° tilt angle, 18 m/s wind speed and 0.9 m rotors distance. The forces and moments have been normalised to the simulated static thrust and torque of the front rotor at of the 100% rotor speed.

5. STATIC LOADS

In this Section, the static loads of the aeroelastic model are compared with the experimental measurements. Then, the numerical model is exploited to analyse conditions different from the ones considered in the wind tunnel.

5.1 Static loads correlation

The measurements of the static loads were subjected to systematic drift which was corrected in post-processing. It was observed that, under fixed environmental conditions and rotor speeds, the load cell measurements exhibited a linear time drift. Additionally, the drift behaviour varied with changes in rotor speed. During the wind tunnel campaign, after setting the configuration and environmental conditions, the LTUs' rotor speeds were increased in steps, with measurements recorded after stabilization. This approach resulted in intervals between measurements without records. The main drawback was the unknown times at which rotor speed changes occurred, leading to consequent changes in static load. To address this issue, a Monte Carlo approach was adopted for each load cell measurement component. By knowing the drift behaviour for two consecutive rotor speeds and the exact times at which measurements were taken, this method considered possible times when rotor speed changes were made. Given a probability distribution for the rotor speed change time, this approach allowed for the calculation of the mean and standard deviation of the static load components, which were then plotted along with a shaded area representing one standard deviation.

Figure 6 presents the normalized measured static forces and moments (blue area) compared to the simulated results (red lines) for both the front and rear LTUs as functions of the rotor speed. The results indicate that the numerical model aligns reasonably well with the measured data. The experimental measurements exhibit an acceptable level of uncertainty for the purposes of this study. Additionally, it was observed that force measurements are more affected by uncertainty compared to moment measurements because the load cell's measurement scale was more suitable for moments and had a higher range for forces. For both LTUs, the longitudinal and lateral forces are negligible relative to the thrust, which is the dominant force. Due to their opposite rotation direction, the two LTUs exhibit approximately opposite rolling moment and torque.

The static load amplitude difference between the two LTUs can be explained as follows. In each LTU, the advancing blade experiences higher dynamic pressure and therefore generates greater lift, causing it to flap upward and reach its peak position near the forward disk location. Conversely, the retreating blade generates a lower lift. As a result, the equivalent disk plane exhibits an elastic pitch-up tilt. Additionally, due to the influence of the front rotor wake, the rear rotor experiences a reduced effective angle of attack, leading to lower thrust and a smaller pitching moment amplitude (with a positive pitching moment indicating a pitch-up).

In the case of an articulated propeller, the blade's response to the free-stream-induced angle of attack would be delayed by about 90°, producing a pure pitch-up tilt. However, for the tested rigid-hub propellers with an elastic blade and high flap frequency, the phase delay is less than 90°, which also introduces a rolling moment. Indeed, at 100%NR the phase delay between pitching moment and rolling moment is around 60°.

The correlation between the measured and simulated static loads was evaluated for all the cases in Table 2, and a good agreement between the experimental and simulated loads was observed. Detailed correlations for different rotor speeds, specifically for the conditions of 0° tilt angle, 18 m/s wind speed, and a rotor separation of 0.7 m are provided in the Appendix.

5.2 Simulated effect of LTUs tilting angle, distance and airspeed on loads

In the previous section, the model was validated using tilting angles between 0° and 20°, LTU distances between 0.7 d/D and 0.9 d/D, and wind speeds of 0 m/s and 18 m/s. In this section, the validated model is used to assess the impact of the LTUs' tilt angle, the distance between LTUs, and wind tunnel airspeed on the static loads. The analysis started with a configuration of a 0° tilt angle, 0.8 m distance between the rotors (d/D = 1.3), and an 18 m/s wind speed. The parameters were then modified one at a time. Figures 7, 8, and 9 show the effects of the tilt angle, LTU distance, and airspeed, respectively.

The tilt angle varied between -20° and 90°. It was observed that transitioning from helicopter mode (tilting 0°, i.e., edgewise flow) to airplane mode (tilting 90°, i.e., axial flow) caused the thrust, rolling moment, and pitching moment of the LTUs to decrease. Indeed, increasing the tilt angle decreases the effective angle of attack until it reaches zero when the tilt angle is about 60°. For tilt angles greater than 60°, the LTUs produce negative lift. When the tilt angle reaches 90°, the forces generated by the blades are independent of the azimuth, generating zero rolling and pitching moments.

The LTU distance was varied between 1.1 d/D and 4 d/D. It was noted that the thrust and pitching moment of the rear LTU increased with distance. As discussed in Section 5.1, the effective angle of attack of the rear propeller is affected by the front rotor wake, whose

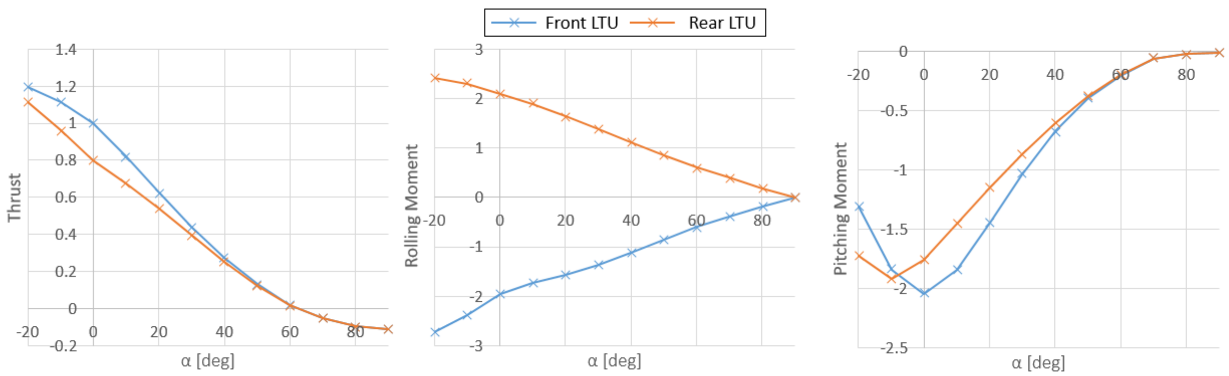

Figure 7: Sensitivity of the tilting angle on the static loads.

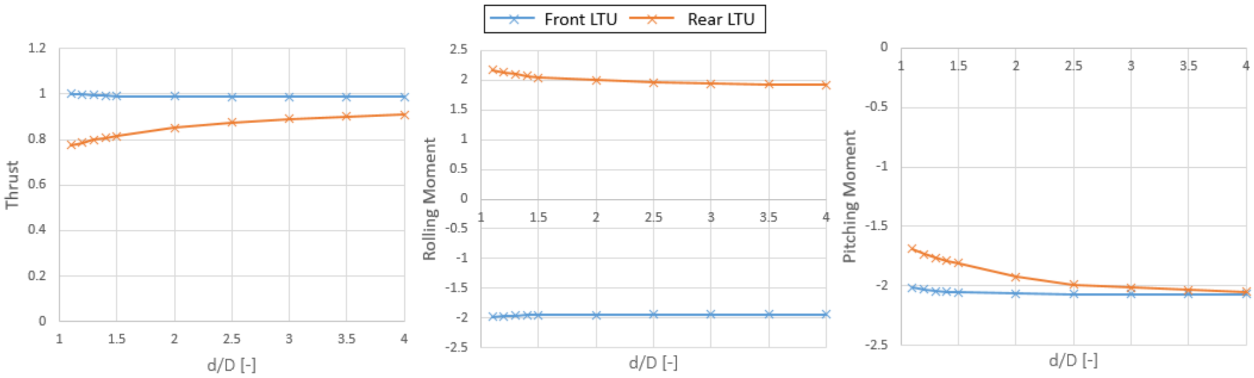

Figure 8: Sensitivity of the LTUs distance on the static loads.

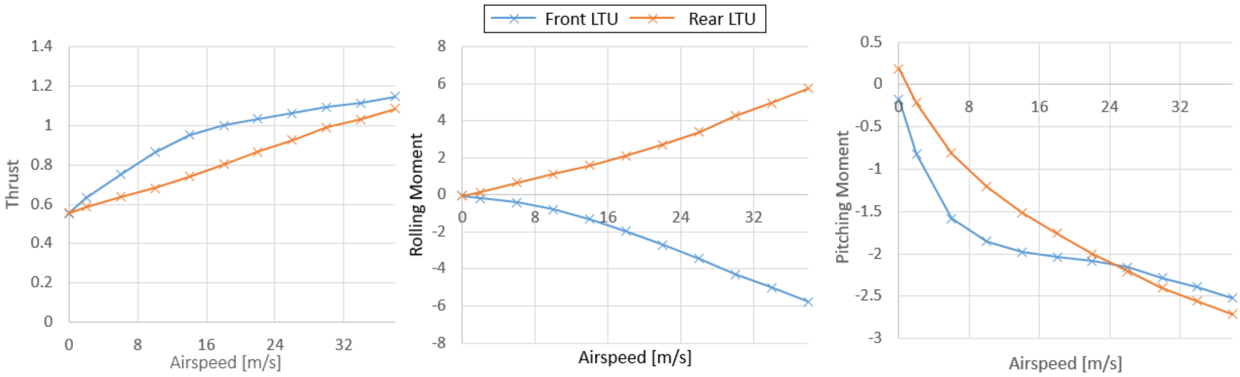

Figure 9: Sensitivity of the airspeed on the static loads.

effect reduces as the distance between the LTUs increases.

The airspeed was varied between 0 m/s and 38 m/s. The results showed that the thrust, rolling moment, and pitching moment of the LTUs increased with airspeed. In Section 5.1, the mechanism behind the disk plane elastic pitch-up tilting was discussed. Increasing the airspeed causes the blade flapping to increase, and consequently, the disk plane pitch-up tilting and the effective incidence angle increase, resulting in higher loads.

The parametric analysis showed that transitioning from helicopter mode (tilting 0°) to airplane mode (tilting 90°), increasing the distance between the LTUs, and operating at both low and high airspeeds resulted in the two LTUs becoming aerodynamically independent. Consequently, the differences between the front and rear LTU disappeared.

6. DYNAMIC LOADS CORRELATION

This section presents preliminary correlation results of the dynamic loads in the z-direction. To improve the correlation, in addition to the LTU model presented in Section 4, the dynamics of the load cell and the structure connecting the LTUs have been introduced into the model. A comprehensive assessment and correlation results for all load components are ongoing and will not be discussed here.

As shown in the scheme of Figure 10, the dynamics of the load cell and the structure connecting the LTUs to the ground were modelled as a sequence of two single degree-of-freedom (SDOF) systems. The two SDOF systems represent the first two mode shapes of the load cell and supporting structure in the z-direction. Zilletti et al. [10] performed a three-dimensional dynamic characterization of the load cell, finding that when excited in the vertical direction (thrust direction), the load cell exhibited a first natural frequency at around 700 Hz. To model this dynamic behaviour, a vertical spring supporting a mass equal to the load cell mass was introduced at the base of each LTU model. The spring was tuned to obtain the measured natural frequency of the load cell at 700 Hz. In addition, based on the natural frequencies and mode shapes in Table 1, the first frame bending mode which significantly contributes to the dynamic response in the z-direction, was considered and modelled as a vertical spring, a vertical damper and a modal mass supporting the load cell. These components were tuned to match the natural frequency and damping ratio of the measured bending mode. In this case, the measured thrust is given by the load across the load cell spring.

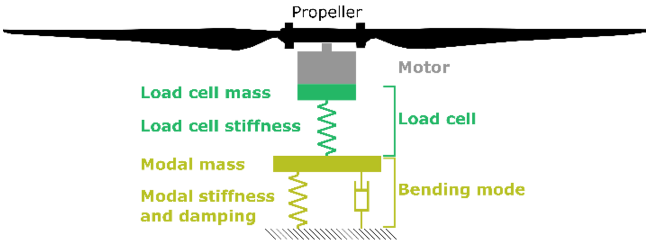

Figure 10: Lumped parameter model of the LTU, load cell and first bending structural mode.

Figure 11 shows the normalized dynamic (3/rev) vertical forces of the front (left plot) and rear (right plot) as a function of the rotor speed with a tilt angle of 0°, 18 m/s wind speed and 0.9 m rotors distance. The black line shows that the measured dynamic thrust is characterised by peaks at various RPM regimes with a dominant peak at about 90% RPM. The blue line shows the simulated dynamic thrust considering only the dynamic model of the LTUs connected to the ground. In this case, the simulated dynamic thrust only shows a peak at around 40% RPM given by the first resonant collective propeller mode and is not able to capture the peak at 90% RPM.

The red lines show the simulated dynamic thrust obtained introducing the dynamic models of the load cell and supporting structure. In this case, in addition to the peak at 40% RPM previously captured by the simpler model of the grounded LTU, the peak at 90% associated with the resonant response of supporting structure is now captured by the model.

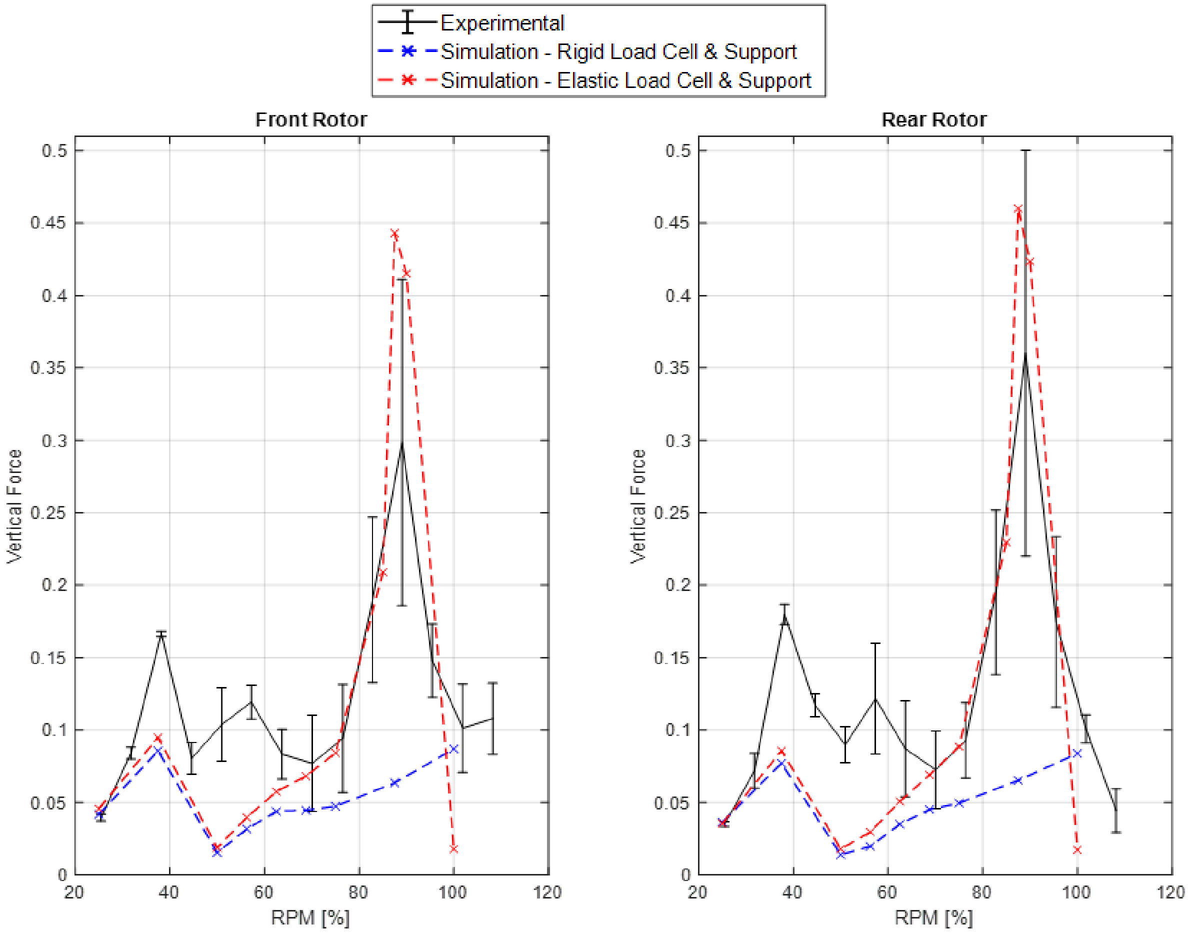

Figure 11: Measured (black line), simulated considering the grounded LTU dynamic models (blue line), and simulated introducing the dynamic models of the load cell and support structure (red line) vertical dynamic forces as a function of the rotor speed. Test condition: 0° tilt angle, 18 m/s wind speed and 0.9 m rotors distance. The forces have been normalised to the simulated static thrust of the front rotor at 100% of the rotor speed.

These results show that high vertical forces can be generated by a rigid propeller exposed to edgewise airflow; the loads at the attachment point of the LTU to the structure can be significantly amplified by the dynamics of the supporting structure. The oscillatory load components are comparable in magnitude with the static ones, potentially generating high vibration levels. The high oscillatory components may have a significant impact on both the sizing of the LTU and its maintainability. These aspects should be considered since the early design stage as they can significantly influence key features of the aircraft, such as control strategies, rotor design, and LTU installation.

CONCLUSIONS

This paper presented the initial results of the wind tunnel testing of two electrical LTUs and their correlation with an aeroelastic model. A test setup was designed and built to characterise the static and dynamic behaviour of electrical LTUs.
The following conclusions can be drawn:

1. An aeroelastic, free wake model implemented using GyroX3 proved to be able to simulate the static and dynamic behaviour of the LTUs in different flight conditions with a satisfactory level of accuracy, compared to the wind tunnel test results.
2. The parametric analysis on the static loads showed that several factors led to the two LTUs becoming aerodynamically independent, thereby eliminating the differences between the front and rear LTUs. These factors include:
    a. Transitioning from helicopter mode (tilting 0°) to airplane mode (tilting 90°).
    b. Increasing the distance between the LTUs.
    c. Operating at both low and high airspeeds.
3. The study confirmed that a stiff rotor can generate high oscillatory loads in edgewise air flow conditions, of magnitude comparable to that of the corresponding static load.
4. The dynamic loads' correlation showed the importance of modelling the LTUs' support structure. Indeed, the introduction of a simplified model of the structure supporting the LTUs has shown to be effective in improving the dynamic correlation. Introducing a tuned single mass-spring-damper system at the base of the LTUs improved the dynamic loads' correlation for a single rotor speed. It is expected that improving the LTU supporting structure model will improve the dynamic correlation for all the rotor speeds and load components.
5. These significant dynamic load levels can impact the sizing and maintainability of the LTU.
6. The high vibratory loads shall be assessed in the early stage of the design as they may suggest the use of alternative design solutions (e.g., variable blade pitch, flapping or teetering blade hinges, LTU tilting, etc.)

Author contact:

Davide Balatti davide.balatti@leonardo.com

REFERENCES

1. Johnson, W., and Silva, C. "NASA concept vehicles and the engineering of advanced air mobility aircraft," The Aeronautical Journal Vol. 126(1295), 2022, pp. 59–91.

2. Silva, Christopher, Wayne R. Johnson, Eduardo Solis, Michael D. Patterson, and Kevin R. Antcliff. "VTOL urban air mobility concept vehicles for technology development." In 2018 Aviation Technology, Integration, and Operations Conference, p. 3847. 2018, Atlanta, Georgia, June 25-29, 2018.

3. Russell C. R. And Sekula M. K., „Comprehensive Analysis Modeling of Small-Scale UAS Rotors" American Helicopter Society 73rd Annual Forum, Fort Worth, Texas, USA, May 2017.

4. Conley, S., "Multirotor Test Bed Load and Stress Analysis" NASA TM 20230000313, 2023.

5. Russell, C., & Conley, S., "The Multirotor Test Bed – A New NASA Test Capability for Advanced VTOL Rotorcraft Configurations" Vertical Flight Society 78th Annual Forum Proceedings, Forth Worth, TX, May 2022.

6. Sekula, M. K., and C. R. Russell, "Time-Frequency Analysis of Experimental and Analytical Hub Loads of a Rotor Undergoing a Rotor Speed Change", Vertical Flight Society 78th Annual Forum Proceedings, Forth Worth, TX, May 2022.

7. Shastry, A., and Datta, A., "Predicting Wake and Structural Loads in RPM Controlled Multirotor Aircraft“ In Vertical Flight Society Aeromechanics for Advanced Vertical Flight Technical Meeting, San Jose, CA, January 2020

8. Staruk, W., Butt, L., Hennig, G., Bonny, E., Gray, C., Represa, D., and Toner, R, "Wind tunnel testing and analysis of a rigid, variable speed rotor for eVTOL applications.“ Journal of the American Helicopter Society 2023.

9. Zilletti, M., D. Prederi, R. Costantini, M. Zaccara, M. Ricciardi, G. Morelli, and P. Masarati. "Wind Tunnel Test of a Single Electrical Lift Thrust Unit to Assess Static and Dynamic Loads." 49th European Rotorcraft Forum (ERF 2023). 2023

10. Sabatino, E., Prederi, D., Petri, F., Sciarappa, A., Cassinelli, C., Frassoldati, G., " Validation of a flexible and highly scalable mid-fidelity aerodynamic solver with wind-tunnel testing", Vertical Flight Society 79th Annual Forum Proceedings, West Palm Beach, FL, May 2023.

Appendix A

Figure A shows the normalized measured (blue area) and simulated (red lines) static forces and moments of the front and rear LTUs as functions of the rotor speed in the case of 0° tilt angle, 18 m/s wind speed and 0.7 m rotors distance.

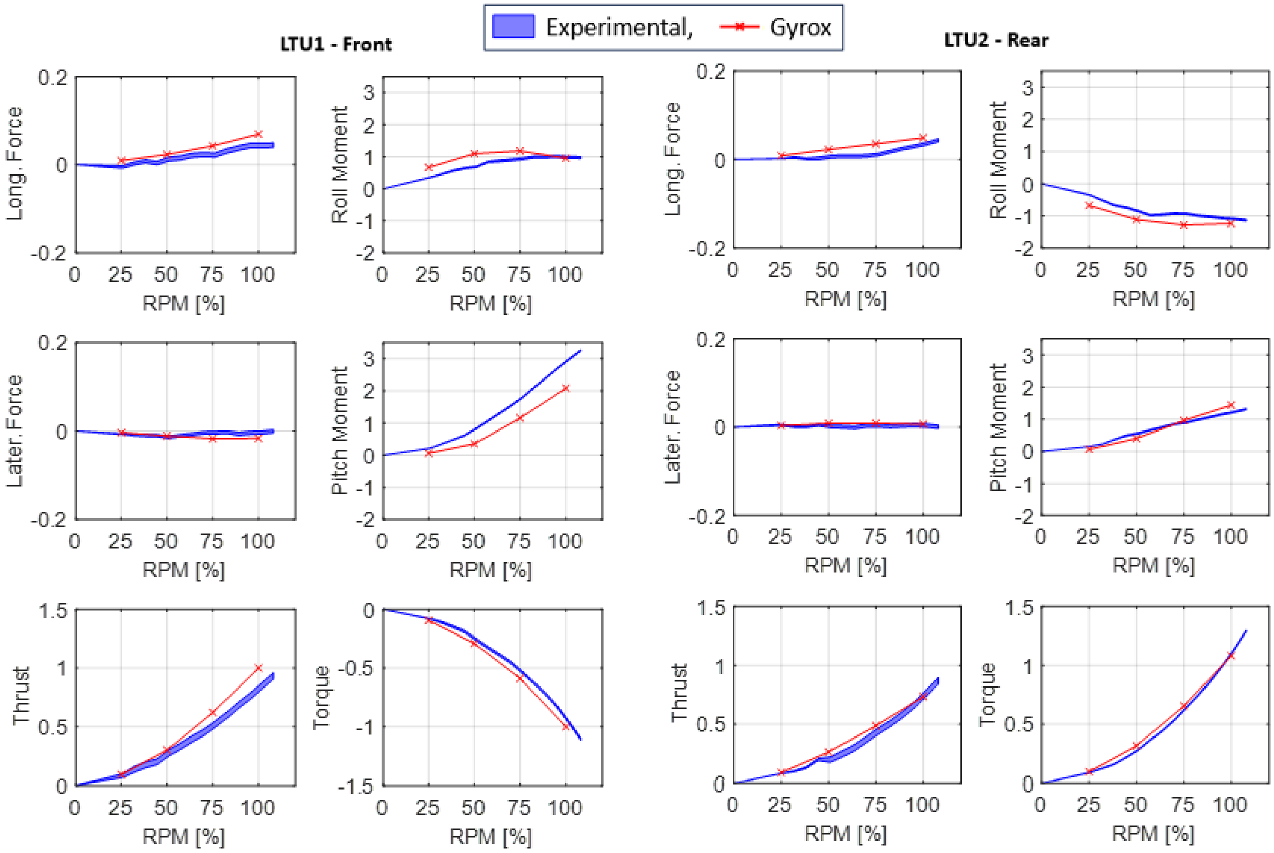

Figure A: Measured (blue area) and simulated (red line) static forces and moments as a function of the rotor speed. Test condition: 0° tilt angle, 18 m/s wind speed and 0.7 m rotors distance. The forces and moments have been normalised to the simulated static thrust and torque of the front rotor at the 100% of the rotor speed.